

High-Performance Hybrid Silicon and Lithium Niobate Mach–Zehnder Modulators for 100 Gbit/s and Beyond

Mingbo He¹, Mengyue Xu¹, Yuxuan Ren², Jian Jian¹, Ziliang Ruan², Yongsheng Xu², Shengqian Gao¹, Shihao Sun¹, Xueqian Wen², Lidan Zhou¹, Lin Liu¹, Changjian Guo², Hui Chen¹, Lei Liu³, Siyuan Yu¹, Liu Liu² and Xinlun Cai¹

¹ State Key Laboratory of Optoelectronic Materials and Technologies and School of Physics and Engineering, Sun Yat-sen University, Guangzhou 510275, China.

² Centre for Optical and Electromagnetic Research, Guangdong Provincial Key Laboratory of Optical Information Materials and Technology, South China Academy of Advanced Optoelectronics, Sci. Bldg. No. 5, South China Normal University, Higher-Education Mega-Center, Guangzhou 510006, China.

Correspondence and requests for materials should be addressed to L.L. (email: liu.liu@coer-scnu.org) or to X. C. (caixlun5@mail.sysu.edu.cn).

Optical modulators are at the heart of optical communication links. Ideally, they should feature low insertion loss, low drive voltage, large modulation bandwidth, high linearity, compact footprint and low manufacturing cost. Unfortunately, these criteria have only been achieved on separate occasions. Based on a Silicon and Lithium Niobate hybrid integration platform, we demonstrate Mach–Zehnder modulators that simultaneously fulfill these criteria. The presented device exhibits an insertion-loss of 2.5 dB, voltage-length product of 1.35 V·cm, electro-optic bandwidth of at least 70 GHz, high linearity and modulation rates up to 112 Gbit/s. The realization of a high-performance modulator is due to seamlessly integration of high-contrast waveguide based on Lithium Niobate - the most mature modulator material - with compact, low-loss silicon circuits. The hybrid platform demonstrated here allows "best-in-breed" active and passive components to be combined and opens up new avenues for future high-speed, energy efficient and cost-effective communication networks.

Global data traffic has witnessed continuous growth with double-digit annual rates over the past three decades due to the insatiable demand of modern society¹. This rapid expansion is placing a serious challenge on the transceivers in all levels of optical networks, i.e., how to significantly increase data rates while reducing energy consumption and cost^{2,3}. To address this challenge, silicon photonics on the silicon-on-insulator (SOI) platform has emerged as the most promising technology due to the possibility of high-quality, low-cost and high-volume production of photonic integrated circuits (PICs) in CMOS foundries, as well as the potential for low-power, high-capacity interconnects on future electronic-photonic integrated circuits (EPICs)^{4,8}.

Silicon optical modulators are key components serving as the information encoding engines from electrical domain to optical domain⁵. Because unstrained silicon does not possess Pockels effect, optical modulation in silicon mainly relies on free-carrier dispersion effect, whereby changes in carrier densities result in changes in the silicon refractive index (RI)⁹⁻¹⁵. Unfortunately, free-carrier dispersion is associated with free-carrier absorption loss which leads to undesired intensity and phase modulation coupling. It also has a nonlinear response to applied voltages. These effects degrade the optical modulation amplitude (OMA) significantly and may lead to signal distortions when using advanced modulation formats.

Tremendous efforts have been made towards realizing high-performance optical modulators in various material platforms¹⁶⁻²⁷. Among them, Lithium Niobate (LN) remains a preferred material due to its excellent physical properties, including a large electro-optic (EO) coefficient (30pm/V), high intrinsic bandwidth and wide transparency window²⁸⁻²⁹. In contrast to silicon, RI of LN responds linearly to the applied electrical field without unwanted residual intensity modulation, which is very appealing for high capacity links. LN modulators show unrivaled results for the generation of high baud rate multilevel signals and are still the best choice for the modulators used in long-haul optical communication links³⁰. Conventional LN modulators are formed by low-index-contrast waveguides with weak optical confinement and the microwave electrodes must be placed far away from the optical waveguide to minimize metal absorption loss, which leads to an increased drive voltage. As a result, conventional LN modulators are bulky in size and low in modulation efficiency ($V_{\pi} L > 10 \text{ V}\cdot\text{cm}$). Recently, LN membranes on insulator (LNOI) has emerged as a promising material platform to increase optical confinement and improve modulation efficiency³⁰⁻⁴³. Waveguides with good confinement have been formed on this platform, either by dry etching or rib-loading with other materials^{35,43}. LNOI modulators with low drive voltage and ultra-high EO bandwidth have been demonstrated^{42,43}.

While significant progress has been made in developing LNOI based optical modulators, an alternative approach, i.e., hybrid integration of LN membranes onto SOI PICs, has also attracted considerable interests⁴⁴⁻⁴⁶. The hybrid silicon/LN material system combines the maturity and scalability of silicon photonics with excellent modulation performance originating from Pockels effect of LN, which is highly desirable from the perspective of optimizing material functionalities. A few demonstrations of hybrid Si/LN optical modulators have been reported, and they all rely on a supermode waveguide structure consisting of an unpatterned LN membrane on top of a silicon waveguide. This structure is designed to support a distributed optical mode that resides in both the LN membrane and the underlying silicon waveguide, i.e. only part of the modal power overlaps with the LN active region, which decreases the modulation efficiency. In fact, the hybrid Si/LN optical modulators demonstrated so far show either low EO bandwidth or high operation voltages, making them difficult to compete with state-of-the-art silicon modulators.

Here, we demonstrate hybrid Si/LN Mach-Zehnder modulators (MZMs) that employ two-layer hybrid integrated waveguides and vertical adiabatic couplers (VACs). The VACs transfer the optical power fully, rather than partially, between the silicon waveguide and LN membrane waveguide. This approach efficiently utilizes the LN membrane and overcomes

the trade-off in the previous approaches. The proposed devices show a large EO bandwidth, high modulation efficiency, low on-chip insertion loss and high linearity. On-off keying (OOK) modulation up to 100 Gbit/s and four-level pulse amplitude modulation (PAM-4) up to 112 Gbit/s are successfully demonstrated in a 3-mm long device.

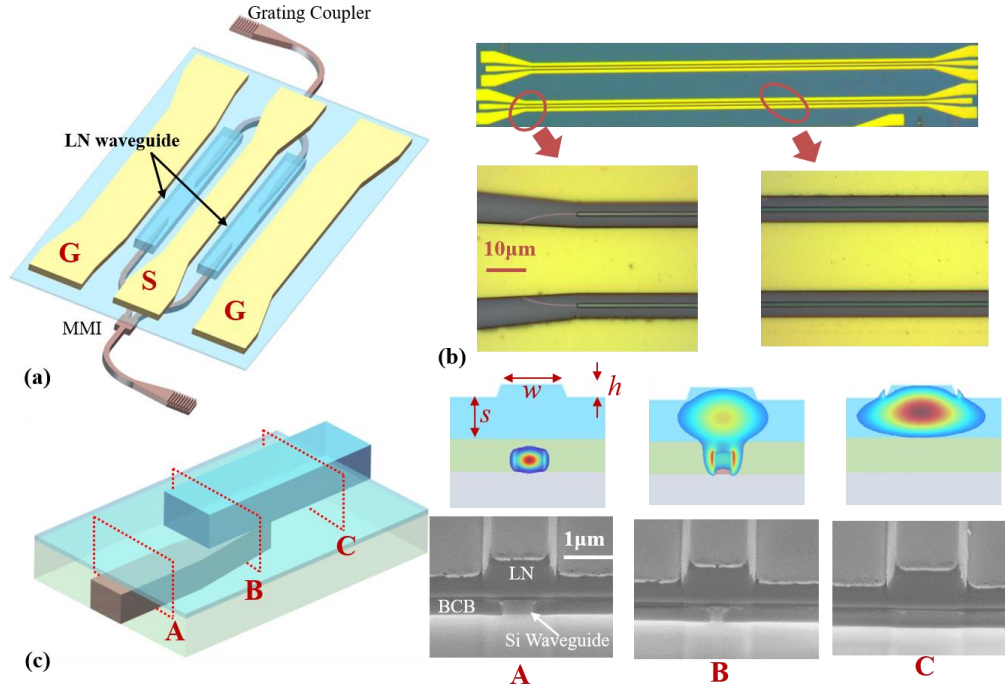


Figure 1 **Structure of the hybrid Si/LN MZM.** (a) Schematic of the structure of the whole circuit. (b) Microscope image of the fabricated devices. (c) Schematic of the vertical adiabatic coupler, scanning electron microscopy images of the cross-sections of the VAC at different positions, and calculated mode distribution associated with the cross-sections.

Results

Design of Hybrid Silicon and LN MZMs. The devices were fabricated based on die-to-wafer bonding technology using benzocyclobuten (BCB) and LN dry etching technique. Fig. 1(a) shows the schematic view of our Si/LN hybrid MZM, consisting of two waveguide layers and VACs. The top waveguides, formed by dry-etching a X-cut LN membrane, serves as phase modulators where EO interactions (Pockels effect) occurs. The bottom SOI circuit supports all other passive functions, and consists of two 3 dB multimode interference (MMI) couplers that split and combine the optical power, and two grating couplers for off-chip coupling. The VACs, which were formed by silicon inverse tapers and superimposed LN waveguides, serve as interfaces to couple light up and down between the two layers. This hybrid integration architecture offers two distinct advantages. Firstly, because task of routing light across the chip is placed on the underlying silicon waveguides, only simple, straight waveguides need to be fabricated in LN membrane. This allows for a more compact device footprint and greater flexibility in the LN waveguide design, compared with that of devices based on pure LNOI platform. Secondly, the VACs, together with dry-etched LN waveguide design, facilitate high overlap between the optical modes and active material, as well as good

optical confinement in LN waveguide. This enables us to exploit the LN active region more efficiently, in contrast to other hybrid Si/LN hybrid devices with unpatterned LN membrane. Optical microscope images of fabricated devices are depicted in Fig. 1(b).

The LN waveguide is the most critical part of the present device, and has to be optimized to enable high modulation efficiency and low optical loss. The fabricated waveguides have a top width of $w = 1 \mu\text{m}$, a rib height of $h = 180 \text{ nm}$, and a slab thickness of $s=420 \text{ nm}$. The gap between the waveguides and electrodes was set to $g=2.25 \mu\text{m}$. These parameters are designed to achieve good balance between the modulation efficiency and optical loss (including both metal absorption and sidewall scattering loss) (Supplementary Section I). The electrodes are configured in a ground-signal-ground (GSG) form, where the two LN waveguides lie in the two gaps between the ground and signal metals. To achieve large EO bandwidth, the electrodes are operated in a traveling wave manner, and optimized for impedance matching, as well as velocity matching of the microwave and light signals (Supplementary Section II). In the present device, the lithography and etching processes were optimized to yield smooth sidewalls and the LN waveguide features a measured propagation loss of 1.16 dB/cm (Supplementary Section III).

The VAC is another important part of the present device (see Fig. 1(c)), and must be optimized for high efficiency. The width of the silicon waveguide tapers from 500 nm to 80 nm over a length of 150 microns , while the width of the LN waveguide remains constant at $1 \mu\text{m}$. The thickness of the BCB is $\sim 300 \text{ nm}$, which is robust enough with respect to the variations induced by the fabrication processes. The measured coupling efficiency of the VAC is $> 90\%$ (-0.42 dB) (Supplementary Section III). Fig. 1(c) presents the electric field patterns for various cross-sections of the VAC, which shows a snap-shot of the process of mode transfer.

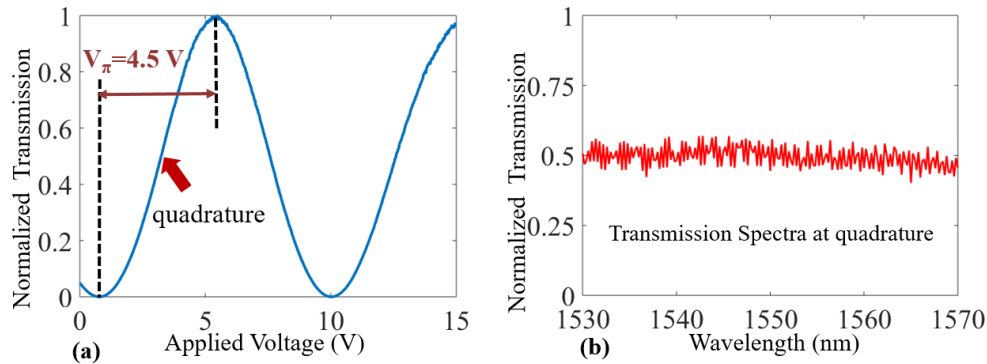


Figure 2 **Static EO Performance.** (a) Optical transmission of a 3 mm long MZM versus the applied DC voltage, indicating a V_π of 4.5 V and voltage-length product of $1.35 \text{ V}\cdot\text{cm}$. (b) Measured transmission spectra of the MZM biased at quadrature, indicating broadband operation of the device.

Static EO Performance. A fabricated MZM device with arm length of 3 mm was measured in detail. The measured on chip optical loss is 2.5 dB (Supplementary Section III). The device is driven in a push-pull configuration, so that applied voltage induces a positive phase shift on one arm and a negative phase shift on the other. Fig.2 (a) shows the optical transmission as a function of the DC applied voltage, and the half-wave voltage V_π is measured to be 4.5 V . This translates to a voltage-length product $V_\pi L$ of $\sim 1.35 \text{ V}\cdot\text{cm}$, which compares favorably to that of silicon modulators operating in depletion mode and is the lowest value to date on any reported LN-based technology to the best of our knowledge. The device also shows an

excellent DC extinction ratio of > 40 dB. Fig.2 (b) shows the measured transmission spectra of the MZM biased at quadrature, indicating broadband operation of the device in the whole C-band. The V_{π} value of the present device can be further reduced by simply increasing the device length, as a LNOI modulator with $V_{\pi}=1.4$ V was recently achieved with a device length of 2 cm^{43} . For the proposed Si/LN hybrid modulator, V_{π} of less than 1 V is expected with the similar length. This would enable small-form factor integration, and driverless modulation from direct CMOS output without comprising the extinction ratio.

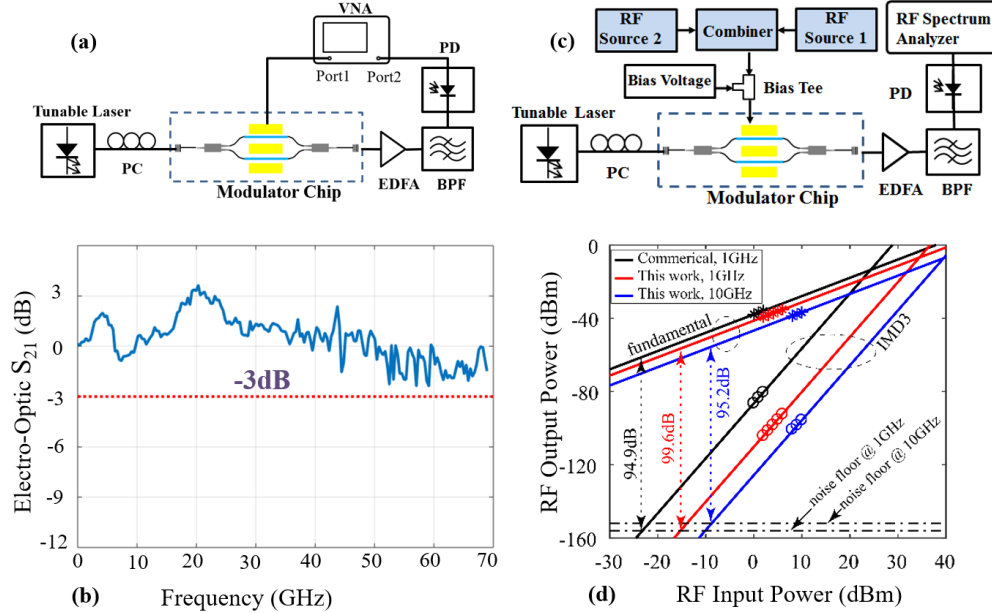


Figure 3 EO Bandwidth and Linearity. (a) Experimental setup for measuring the EO bandwidth. VNA, vector network analyzer; EDFA, erbium-doped fiber amplifier; BPF, band-pass filter; PD, photodetector; PC, polarization controller. (b) EO bandwidths (S_{21} parameter) of a 3-mm long MZM. The modulation response decays to 1.8 dB at 67 GHz, and the 3 dB bandwidth is beyond the measurement limit of the VNA. (c) Experimental setup for measuring the IMD3 SFDR. (d) RF output power of the fundamental and IMD3 components as a function of RF input power for our device at 1 GHz and 10 GHz, and for a commercially available LN MZM at 1 GHz. The noise floor is in 1 Hz bandwidth, limited by the RF spectral analyzer.

EO Bandwidth and Linearity. We then characterized the small signal EO bandwidth (S_{21} parameter) of the fabricated device using the setup shown in Fig. 3(a). The measured 3-dB EO bandwidth is > 70 GHz, which is beyond the measurement limits of our vector network analyzer (VNA). The measured EO bandwidth is much higher than that of pure silicon based modulators. We believe that the EO bandwidth of the present device could be extend beyond 100GHz by further optimizing the travelling-wave electrode (Supplementary Section II).

To characterize the linearity of the present device, we further examine the third order intermodulation (IMD3) spurious free dynamic range (SFDR) performance using the setup shown in Fig. 3 (c). To provide a comparative study, we also measured the IMD3 SFDR of a commercially available LN MZM (Fujitsu) with the same measurement system. Both devices

are biased at quadrature and the optical power reaching the photodetector after pre-amplification is kept at 0 dBm. For our device, the measured IMD3 SFDR is 99.6 dB Hz^{2/3} at 1 GHz, which is slightly better than that achieved by the commercial LN MZM (94.9 dB Hz^{2/3}). At 10 GHz, the measured SFDR decreases slightly to 95.2 dB Hz^{2/3}, mainly due to the higher noise floor of the measurement system. The SFDR value can be increased further by increasing the received optical power.

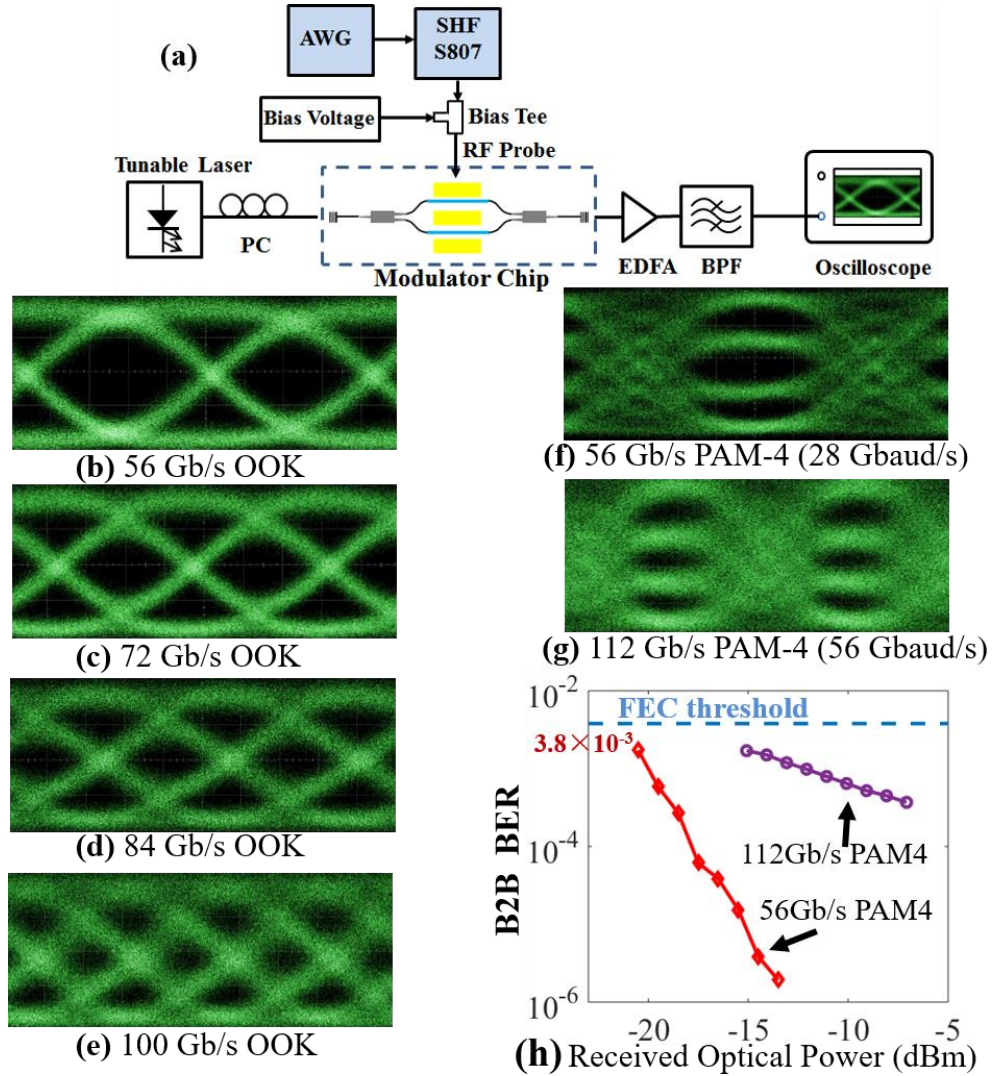


Figure 4 **Data Transmission Testing.** (a) Experimental setup for measuring the eye diagram. AWG, arbitrary waveform generator. (b-e) Optical eye diagrams at data rates of 56 GBaud/s, 72 GBaud/s, 84 GBaud/s, and 100 GBaud/s. The dynamic extinction ratios are 11.8 dB, 6.0 dB, 5.5 dB and 5.0 dB, respectively. (f-g) Measured PAM-4 modulation optical eye diagrams at 28 GBaud/s and 56 GBaud/s. (h) Measured curve of BER versus the received optical power for 28 GBaud/s (56 Gb/s) and 56 GBaud/s (112 Gb/s) PAM-4 signal.

Data Transmission Testing. Next, we evaluated the performance of the present modulator for high-speed digital data transmission, as depicted in Fig. 4 (a). First, the OOK modulations were applied to the device. Fig. 4 (b-e) summarizes the optical eye diagrams at 56, 72, 84 and 100 GBaud/s. The measured extinction ratios are 11.8, 6.0, 5.5 and 5.0 dB, respectively. It is noteworthy that at 100 GBaud/s the whole measurement system is already limited by the bandwidth of the RF probe and cables. PAM-4 experiments were also carried out with the same experimental setup. The optical PAM-4 eye-diagrams at 28 GBaud/s and 56 GBaud/s are shown in Fig. 4 (f-g). The bit-error rate curves at both PAM-4 data rates, shown in Fig. 4 (h), present linear decreases as the received optical power before pre-amplification increases. No error floor is observed in the measured power range, and the error rates are also well below the hard-FEC limit of 3.8×10^{-3} .

Discussion

As discussed above, the hybrid Si/LN MZMs demonstrated here can achieve excellent optical modulation characteristics, while maintaining the key advantages of SOI photonic circuits. LN active waveguides can be bonded and fabricated with lithographic precision and alignment accuracy, in a back-end process after the SOI fabrication. This manufacturing procedure is highly scalable and fully CMOS-compatible. Therefore, our approach potentially provides a new generation of compact, high performance optical modulators for telecommunications and data-interconnects.

It should be noted that approaches of combining silicon with other materials exhibiting Pockels effects, such as organic materials and barium titanate (BTO), have also been investigated. In Table 1, we compare the performance of the present device with state-of-the-art, including silicon-organic-hybrid (SOH) MZMs, SOH plasmonic MZMs, and BTO/Si plasmonic MZMs. Here, we focus on MZMs with either large EO bandwidth or high operation speed, and results of pure silicon modulator operating in carrier depletion mode is also included as a benchmark. As shown in Tab. 1, the present device in this work is the only one, on which low V_π and low insertion loss are achieved simultaneously. In particular, the insertion loss of the present device is much lower than that of all others. The demonstrated V_π of the present device is also promising, which is only surpassed by the SOH modulator with a much higher insertion loss. As discussed above, the V_π can be further engineered to be less than 1 V while keeping an insertion loss of less than 4 dB.

The underlying silicon waveguides not only route light with low losses across the chip, but also allow integration of the present modulator with the complete suite of silicon photonic components. This makes the proposed Si/LN platform highly desirable for new emerging applications. For instance, future integrated microwave photonic (MWP) systems would require on-chip linear modulators featuring high-fidelity electronic-to-optical conversion. The present device is ideal for this scenario and can be envisaged to be co-integrated with passive SOI structures, such as Bragg gratings or micro-resonators, to form sophisticated integrated MWP circuits. Another possible application area could be linear optical quantum computing (LOQC)⁵⁰. LOQC relies on universal quantum gates which could be implemented by adding auxiliary photons and by using rapid, time-of-flight feedforward. In practice, a feedforward step requires large-scale, low loss, rapidly reconfigurable (in GHz range) optical circuits capable of low-noise pure phase modulation – requirements that are attainable on our platform. The present platform is also amenable to further integration with lasers and detectors offering fully integrated solutions for future terabit-per-second datacom and interconnect applications. The fabrication process can also be adapted for materials such as Si_3N_4 , which enables ultra-low loss PICs and potential platform for exploring nonlinear optical processes.

Table 1 Comparison of several performance metrics for hybrid silicon MZM

	Loss	V_{π}	EO Bandwidth	OOK Data Rate
SOI ¹⁰	5.4 dB	7 V	58 GHz	90 Gb/s (3.3 dB ER)
SOH ²¹	11 dB	22 V	>100 GHz	N.A.
SOH ⁴⁷	11 dB	0.9 V	25 GHz	100 Gb/s (5.7 dB ER)
SOH Plasmonic ⁴⁸	12 dB	>40 V	>65 GHz	40 Gb/s
Si/BTO Plasmonic ⁴⁹	30 dB	25 V	>100 GHz	72 Gb/s
This Work	2.5 dB	4.5 V	>70 GHz	100 Gb/s (5.0 dB ER)

Method

Fabrication: A standard SOI processing including e-beam lithography (EBL) and dry etching processes were used to fabricate the grating coupler, 3dB MMIs, and silicon inverse tapers. A LN on insulator sample with silicon substrate was flip-bonded to the SOI wafer using BCB adhesive bonding process. The substrate of the LNOI was removed by mechanical grinding and dry etching. Afterward, the LN waveguide was patterned by EBL and dry etching process. Finally, the travelling wave electrode was patterned through liftoff process.

Dynamic measurement: The setup for EO bandwidth, linearity, and data transmission measurements are shown in Fig. 2, 3, 4 respectively. The electrical signal is fed to the device electrode through a 67GHz RF probe (GGB 67A). The second RF probe (not shown) is also attached to the end of the travelling wave electrode, and a 50ohm termination is applied to the probe for impedance matching. For the optical signal, light from a tunable laser is coupled into and collected from the SOI grating coupler using single mode fibers. A polarization controller is used to ensure TE input polarization. The received optical signal is pre-amplified and filtered through an erbium-doped fiber amplifier (EDFA) and a band-pass filter (BPF) before detection. For bandwidth measurement, a VNA is used to analyze the electrical signal, and the frequency response of the PD (XPDV4120R) is deducted from the measured S21 response. For linearity measurement, the input electrical signal consists of a DC bias and two RF tones with frequencies separated by 10MHz and centered at the desired frequency. An RF spectrum analyzer is used to analyze frequency components of the received electrical signal. For data transmission measurement, an arbitrary waveform generator (AWG, Micram) with 100Gs/s sampling rate is used to generate the electrical signals. A 50 GHz broadband amplifier (SHF 807) with output saturation V_{pp} of 5 V is used to amplify the driving signal to the modulator together with a DC bias. For PAM-4 eye diagram measurements, the levels of the driving signals are deducted from an inverse trigonometric function in order to compensate the typical sinusoid response of the MZI. Digital low-pass filters are also applied to limit the signal bandwidth. For the bit-error rate measurements, the detected signal is sampled by a real-time oscilloscope, and analyzed using an off-line DSP, including resampling, equalization, and symbol decision.

References

1. Cisco. Cisco Visual Networking Index: Forecast and Methodology, 2015–2020, (2016).

2. R. W. Tkach. Scaling optical communications for the next decade and beyond. *Bell Labs Tech. J.* 14, 3–10 (2010).
3. D. C. Kilper and H. Rastegarfar. Energy challenges in optical access and aggregation networks. *Phil. Trans. R. Soc. A.* 374, 20140435 (2016).
4. D. A. B. Miller. Device requirements for optical interconnects to silicon chips. *Proc. IEEE.* 97, 1166–1185 (2009).
5. G. T. Reed, G. Mashanovich, F. Y. Gardes & D. J. Thomson. Silicon optical modulators. *Nat. Photon.* 4, 518–526 (2010).
6. M. J. Heck, H. Chen, A. W. Fang, B. R. Koch, D. Liang, H. Park, M. N. Sysak & J. E. Bowers. Hybrid silicon photonics for optical interconnects. *IEEE J. Sel. Top. Quantum Electron.* 17, 333–346 (2011).
7. W. Bogaerts, R. Baets, P. Dumon, V. Wiaux, S. Beckx, D. Taillaert, B. Luyssaert, J. Van Campenhout, P. Bienstman, & D. Van Thourhout. Nanophotonic Waveguides in Silicon-on-Insulator Fabricated with CMOS Technology. *J. Lightwave Technol.* 23, 401–412 (2005).
8. Sun C, Wade M T, Lee Y, et al. Single-chip microprocessor that communicates directly using light. *Nature* 528, 534–538 (2015).
9. Q. Xu, B. Schmidt, S. Pradhan, & M. Lipson. Micrometre-scale silicon electro-optic modulator. *Nature* 435, 325–327 (2005).
10. M. Li, L. Wang, X. Li, X. Xiao, & S. Yu. Silicon intensity Mach–Zehnder modulator for single lane 100 Gb/s applications. *Photon. Research* 6, 109–116 (2018).
11. L. Chrostowski & M. Hochberg, *Silicon Photonics Design: From Devices to Systems* (Cambridge University, Cambridge, England, 2015).
12. R. Ding, Y. Liu, Y. Ma, Y. Yang, Q. Li, A. E.-J. Lim, G.-Q. Lo, K. Bergman, T. Baehr-Jones & M. Hochberg. High-speed silicon modulator with slow-wave electrodes and fully independent differential drive. *J. Lightwave Technol.* 32, 2240–2247 (2014).
13. P. Dong, X. Liu, S. Chandrasekhar, L. L. Buhl, R. Aroca & Y.-K. Chen. Monolithic silicon photonic integrated circuits for compact 100+ Gb/s coherent optical receivers and transmitters. *IEEE J. Sel. Top. Quantum Electron.* 20, 150–157 (2014).
14. A. Samani, D. Patel, M. Chagnon, E. Elfiky, R. Li, M. Jacques, N. Abadia, V. Veerasubramanian, & D. V. Plant. Experimental parametric study of 128 Gb/s PAM-4 transmission system using a multielectrode silicon photonic Mach Zehnder modulator. *Opt. Express* 25, 13252–13262 (2017).
15. E. Timurdogan, C. M. Sorace-Agaskar, J. Sun, E. Shah Hosseini, A. Biberman & M. R. Watts. An ultralow power athermal silicon modulator. *Nat. Commun.* 5, 4008 (2014).
16. C. Xiong, W. H. P. Pernice, X. Sun, C. Schuck, K. Y. Fong & H. X. Tang. Aluminum nitride as a new material for chip-scale optomechanics and nonlinear optics. *New J. Phys.* 14, 095014 (2012).
17. C. Zhang, P. A. Morton, J. B. Khurgin, J. D. Peters & J. E. Bowers. Ultralinear heterogeneously integrated ring-assisted Mach-Zehnder interferometer modulator on silicon. *Optica* 3, 1483–1488 (2016).
18. Y. Tang, H.-W. Chen, S. Jain, J. D. Peters, U. Westergren & J. E. Bowers. 50 Gb/s hybrid silicon traveling-wave electroabsorption modulator. *Opt. Express* 19, 5811–5816 (2011).

19. C. Haffner, W. Heni, Y. Fedoryshyn, J. Niegemann, A. Melikyan, D. L. Elder, B. Baeuerle, Y. Salamin, A. Josten, U. Koch, C. Hoessbacher, F. Ducry, L. Juchli, A. Emboras, D. Hillerkuss, M. Kohl, L. R. Dalton, C. Hafner & J. Leuthold. All-plasmonic Mach-Zehnder modulator enabling optical high-speed communication at the microscale. *Nat. Photon.* 9, 525–528 (2015).
20. Christian Haffner, Daniel Chelladurai, Yuriy Fedoryshyn, Arne Josten, Benedikt Baeuerle, Wolfgang Heni, Tatsuhiko Watanabe, Tong Cui, Bojun Cheng, Soham Saha, Delwin L. Elder, Larry. R. Dalton, Alexandra Boltasseva, Vladimir M. Shalaev, Nathaniel Kinsey & Juerg Leuthold. Low-loss plasmon-assisted electro-optic modulator. *Nature* 556, 483–486 (2018).
21. L. Alloatti, R. Palmer, S. Diebold, K. P. Pahl, B. Chen, R. Dinu, M. Fournier, J.-M. Fedeli, T. Zwick, W. Freude, C. Koos & J. Leuthold. 100 GHz silicon-organic hybrid modulator. *Light: Science and Applications*. 3, e173 (2014).
22. M. Lee, H. E. Katz, C. Erben, D. M. Gill, P. Gopalan, J. D. Heber & D. J. McGee. Broadband modulation of light by using an electro-optic polymer. *Science* 298, 1401–1403 (2002).
23. Jae-Hoon Han, Frederic Boeuf, Junichi Fujikata, Shigeki Takahashi, Shinichi Takagi & Mitsuru Takenaka. Efficient low-loss InGaAsP/Si hybrid MOS optical modulator. *Nat. Photon.* 11, 486–490 (2017)
24. N. Kikuchi, E. Yamada, Y. Shibata & H. Ishii. High-Speed InP-Based Mach-Zehnder Modulator for Advanced Modulation Formats. In *Compound Semiconductor Integrated Circuit Symposium 1–4* (IEEE, 2012).
25. C. T. Phare, Y.-H. Daniel Lee, J. Cardenas & M. Lipson. Graphene electro-optic modulator with 30GHz bandwidth. *Nat. Photon.* 9, 511–514 (2015).
26. M. Liu, X. Yin, E. Ulin-Avila, B. Geng, T. Zentgraf, L. Ju, F. Wang & X. Zhang. A graphene-based broadband optical modulator. *Nature* 474, 64–67 (2011).
27. V. Sorianoello, M. Midrio, G. Contestabile, I. Asselberghs, J. Van Campenhout, C. Huyghebaert, I. Goykhman, A. K. Ott, A. C. Ferrari & M. Romagnoli. Graphene-silicon phase modulators with gigahertz bandwidth. *Nat. Photon.* 12, 40–44 (2018).
28. Antao Chen & Edmond J. Murphy. *Broadband Optical Modulators: Science, Technology, and Applications* (CRC Press, Boca Raton, U.S.A, 2011).
29. E. L. Wooten, K. M. Kissa, A. Yi-Yan, E. J. Murphy, D. A. Lafaw, P. F. Hallemeier, D. Maack, D. V. Attanasio, D. J. Fritz, G. J. McBrien & D. E. Bossi. A review of lithium niobate modulators for fiber-optic communications systems. *IEEE J. Sel. Top. Quantum Electron.* 6, 69–82 (2000).
30. G. Raybon, J. Cho, A. Adamiecki, P. Winzer, A. Konczykowska, F. Jorge, J.-Y. Dupuy, M. Riet, B. Duval, K. Kim, S. Randel, D. Pileri, B. Guan, N. Fontaine & E. C. Burrows. Single Carrier High Symbol Rate Transmitter for Data Rates up to 1.0 Tb/s. In *Optical Fiber Communication Conference Th3A-2* (OSA, 2016).
31. D. Janner, D. Tulli, M. Garcia-Granda, M. Belmonte & V. Pruneri. Micro-structured integrated electro-optic LiNbO₃ modulators. *Laser Photonics Rev.* 3, 301–313 (2009).
32. G. Poberaj, H. Hu, W. Sohler & P. Günter. Lithium niobate on insulator (LNOI) for micro-photonic devices. *Laser Photonics Rev.* 6, 488–503 (2012).
33. A. Guarino, G. Poberaj, D. Rezzonico, R. Degl’Innocenti & P. Günter. Electro-optically tunable microring resonators in lithium niobate. *Nat. Photon.* 1, 407–410 (2007).

34. S. Jin, L. Xu, H. Zhang & Y. Li. LiNbO₃ thin-film modulators using silicon nitride surface ridge waveguides. *IEEE Photonics Technol. Lett.* 28, 736–739 (2016).
35. A. Rao, A. Patil, P. Rabiei, A. Honardoost, R. DeSalvo, A. Paoletta & S. Fathpour. High-performance and linear thin-film lithium niobate Mach-Zehnder modulators on silicon up to 50GHz. *Opt. Lett.* 41, 5700–5703 (2016).
36. J. Wang, F. Bo, S. Wan, W. Li, F. Gao, J. Li, G. Zhang & J. Xu. High-Q lithium niobate microdisk resonators on a chip for efficient electro-optic modulation. *Opt. Express* 23, 23072–23078 (2015).
37. L. Cai, Y. Kang & H. Hu. Electric-optical property of the proton exchanged phase modulator in single-crystal lithium niobate thin film. *Opt. Express* 24, 4640–4647 (2016).
38. M. Wang, Y. Xu, Z. Fang, Y. Liao, P. Wang, W. Chu, L. Qiao, J. Lin, W. Fang & Y. Cheng. On-chip electro-optic tuning of a lithium niobate microresonator with integrated in-plane microelectrodes. *Opt. Express* 25, 124–129 (2017).
39. C. Wang, M. J. Burek, Z. Lin, H. A. Atikian, V. Venkataraman, I. C. Huang, P. Stark & M. Lončar. Integrated high quality factor lithium niobate microdisk resonators. *Opt. Express* 22, 30924–30933 (2014).
40. L. Chang, Y. Li, N. Volet, L. Wang, J. Peters & J. E. Bowers. Thin film wavelength converters for photonic integrated circuits. *Optica* 3, 531–535 (2016).
41. L. Chang, M. H. P. Pfeiffer, N. Volet, M. Zervas, J. D. Peters, C. L. Manganelli, E. J. Stanton, Y. Li, T. J. Kippenberg & J. E. Bowers. Heterogeneous integration of lithium niobate and silicon nitride waveguides for wafer-scale photonic integrated circuits on silicon. *Opt. Lett.* 42, 803–806 (2017).
42. Cheng Wang, Mian Zhang, Brian Stern, Michal Lipson & M. Lončar. Nanophotonic lithium niobate electro-optic modulators. *Opt. Express* 26, 1547–1555 (2018).
43. Cheng Wang, Mian Zhang, Xi Chen, Maxime Bertrand, Amirhassan Shams-Ansari, Sethumadhavan Chandrasekhar, Peter Winzer & M. Lončar. Ultra-High Bandwidth Integrated Lithium Niobate Modulators with Record-Low Vp. In *Conference on Optical Fiber Communications Th4A.5* (OSA, 2018).
44. L. Chen, M. G. Wood & R. M. Reano. 12.5 pm/V hybrid silicon and lithium niobate optical microring resonator with integrated electrodes. *Opt. Express* 21, 27003–27010 (2013).
45. L. Chen, Q. Xu, M. G. Wood & R. M. Reano. Hybrid silicon and lithium niobate electro-optical ring modulator. *Optica* 1, 112–118 (2014).
46. Peter O.Weigel. et al. Hybrid Silicon Photonic-Lithium Niobate Electro-Optic Mach-Zehnder Modulator Beyond 100 GHz Bandwidth. Preprint at <https://arxiv.org/abs/1803.10365> (2018).
47. S. Wolf, et al. Silicon-Organic Hybrid (SOH) Mach-Zehnder Modulators for 100 Gbit/s On-Off Keying. *Scientific Report* 8, 2598 (2018).
48. A. Melikyan, et al. High-speed plasmonic phase modulators. *Nat. Photon.* 8, 229–233, (2014).
49. A. Messner, et al. Integrated Ferroelectric BaTiO₃/Si Plasmonic Modulator for 100 Gbit/s and Beyond. In *Optical Fiber Communication Conference M2I.6* (OSA, 2018).
50. Pieter Kok, W. J. Munro, Kae Nemoto, T. C. Ralph, Jonathan P. Dowling, and G. J. Milburn, Linear optical quantum computing with photonic qubits. *Rev. Mod. Phys.* 79, 135, (2007).